2014 IEEE International Conference on Robotics & Automation (ICRA)
Hong Kong Convention and Exhibition Center
May 31 - June 7, 2014. Hong Kong, China

Attitude-Guided Robust Adaptive Path Following Control for Ducted Fan UAV

Yanhe Zhu, Ge Li, Jie Zhao, and Hongzhe Jin

***Abstract*—This article presents an approach and a systematic design methodology to path following control based on motion decoupling for high-performance ducted fan unmanned aerial vehicles (UAVs). The decoupling is performed according to the principle of regarding the attitude motion as a virtual input of the lateral longitudinal flight dynamics. This allows the attitude and flight controllers to be designed individually without mutual interference. Considering that dynamics of the ducted fan UAV is uncertain, an estimation method of system function based on the smooth saturation function and the state variable integral is proposed. This method has the advantage of less computation while keeping the high estimation performance. The stability analysis and the simulation results showing the practical feasibility of the proposed control scheme to ducted fan UAVs are given.**

I. Introduction

The ducted fan UAV has gained increasing interest among professional researchers for its high propulsion efficiency [1]. To avoid the adverse effects of the gyroscopic couplings, the coaxial dual-propellers and the control surface having a large lift-to-drag ratio are used in the actuate system design. These characteristics show that the ducted fan UAV possesses a great potential in the high-altitude surveillance.

The ducted fan UAV is a nonlinear under-actuated system, the attitude and flight dynamics of which share the control inputs generated by the control surfaces and highly couple with each other. The technique of the dynamic-inversion plays an important role in dealing with the control framework of this kind of system [2]—[4]. Original system dynamic equation is transformed into a linear equation via feedback linearization, so as to simplify the controller design. However, an accurate modeling for the ducted fan UAV is necessary for the dynamic inversion control.

Recently, the issue of enhancing the system robustness has come into focus, among which, the theories on neural network and robust adaptive control have been successfully applied to the technique of the ducted fan UAV and have been verified to be reliable and efficient in overcoming the adverse effects of the unknown disturbances including the modeling errors [5]—[8]. However, the relatively large amount of calculation is needed to update the weight coefficients of the activation functions for neural-network-based intelligent controllers. As regards adaptive controllers, the estimation process of every system parameter highly relies on the structural information of the system function.

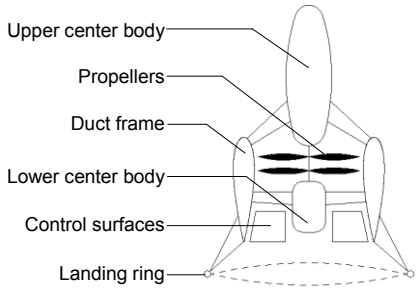

Fig. 1 A view of ducted fan UAV [7]

This article presents a novel decoupling control framework for the path following of ducted fan UAVs. The behaviors of flight and attitude dynamics are decoupled well by proposing the following design procedures: 1) constructs the pseudo control inputs in the lateral and longitudinal flight dynamics; 2) imports their values into an attitude command generator, which is designed by using the inverse kinematics of ducted fan UAV; 3) designs a controller for the attitude command tracking, which generates an attitude matching with the path following. This decoupling approach enables the ducted fan UAV to follow the desired path well by the attitude-guidance, even though the ducted fan UAV turns about its yaw axis.

Given the dynamics of the ducted fan UAV is uncertain, in the controller design, an estimation approach of the system function is proposed based on the state variable integral and the smooth saturation function. This approach differs from the schemes mentioned previously in that the system function is considered as a disturbance composed of the low and high frequency components, whose values are easy to be estimated by the adaptive adjustments for the integral gain and for the weight coefficient of the saturation function. Therefore, both a high efficiency in the algorithm calculations and the correct compensation on the unknown disturbance are realized.

The remainder of this article is organized as follows. The dynamics of ducted fan UAV is described in Section II. The design scheme of the proposed controller and its associated stability analysis are discussed in Section III and Section IV. Simulation results are described in Section V to illustrate the proposed concept. Section V contains concluding remarks.

Manuscript received September 15, 2013. This work was supported by the National Natural Science Foundation of China (Grant No. 61004076), Postdoctoral Science Foundation of China (Grant No. 20100480995), Research Fund for the Doctoral Program of Higher Education of China (Grant No. 20102302120041), and Self-Planned Task of State Key Laboratory of Robotics and System (HIT, No. SKLRS200902B).

Authors are with the Harbin Institute of Technology, Harbin, China (corresponding author: Hongzhe Jin; phone: +86-451-86413382; fax: +86-451-86414538; e-mail: hongzhejin@hit.eud.cn)

II. MODELING

A. Kinematics

Two reference frames are considered to describe dynamics of ducted fan UAV: I is an inertial frame attached to the earth and A is a body-fixed frame attached to the center of mass of ducted fan UAV. The position of center of mass of ducted fan UAV with respect to I and the angular velocity of ducted fan UAV with respect to A are expressed as $\mathbf{\Xi}=[\,x\ \ y\ \ z\,]^T$ and $\mathbf{\Omega}=[\,\omega_x\ \ \omega_y\ \ \omega_z\,]^T$, respectively. The attitude $\mathbf{R}=[r_{ij}]$ (i =1, 2, 3, j =1, 2, 3) of A with respect to I is represented by means of the Euler angles: $\mathbf{\Theta}=[\,\theta\ \ \psi\ \ \phi\,]^{\mathrm{T}}$ (θ: pitch angle, ψ : roll angle, ϕ : yaw angle).

The relation between $\mathbf{\Omega}$ and $\dot{\mathbf{\Theta}}$ is given as follows:

$$\mathbf{\Omega}=\mathbf{Q}\dot{\mathbf{\Theta}} \tag{1}$$

where $\mathbf{Q}=\begin{bmatrix} 0 & 1 & -\sin\theta \\ \cos\psi & 0 & \cos\theta\sin\psi \\ -\sin\psi & 0 & \cos\theta\cos\psi \end{bmatrix}$.

B. Forces Acting on the Ducted Fan UAV

The control force $\mathbf{F_c}$ with respect to A, the aerodynamic drag $\mathbf{F_d}$ with respect to I, and the gravity $\mathbf{F_g}$ of ducted fan UAV with respect to I are expressed as

$$\mathbf{F_c}=\begin{bmatrix} f_1+f_3 \\ f_2+f_4 \\ f_t \end{bmatrix}\triangleq\begin{bmatrix} f_c^x \\ f_c^y \\ f_c^z \end{bmatrix},\ \mathbf{F_d}=\begin{bmatrix} c_x|v_x|v_x \\ c_y|v_y|v_y \\ c_z|v_z|v_z \end{bmatrix}\triangleq\begin{bmatrix} f_x^d \\ f_y^d \\ f_z^d \end{bmatrix},\ \mathbf{F_g}=\begin{bmatrix} 0 \\ 0 \\ mg \end{bmatrix},$$

where f_1, f_2 $\cdots$, and f_4 are the aerodynamic lifts of the four control surfaces, f_t is the propeller thrust, c_x, c_y, and c_z are the aerodynamic drag coefficients, v_x, v_y, and v_z are the relative velocities between the ducted fan UAV and the external airstream, m is the mass of ducted fan UAV, and g is the acceleration of gravity.

C. Torques Acting on the Ducted Fan UAV

The control torque $\mathbf{T_c}$ with respect to A satisfies the following equation [6, 7]:

$$\mathbf{T_c}=\begin{bmatrix} (f_2+f_4)l_1 \\ (f_1+f_3)l_1 \\ (f_1-f_3+f_2-f_4)l_2 \end{bmatrix}\triangleq\begin{bmatrix} \tau_x \\ \tau_y \\ \tau_z \end{bmatrix}$$

where l_1 is the distance between the origin of A and the center of mass of the steering engine composed of four control surfaces, and l_2 is the distance between the center of mass of steering engine and the center of mass of each control surface. From this relation, we obtain

$$f_2=\frac{\tau_x}{2l_1}+\frac{\tau_z}{4l_2},\ f_4=\frac{\tau_x}{2l_1}-\frac{\tau_z}{4l_2},$$

$$f_1=\frac{\tau_y}{2l_1}+\frac{\tau_z}{4l_2},\ f_3=\frac{\tau_y}{2l_1}-\frac{\tau_z}{4l_2}.$$

In the reference frame defined by Euler angles, the control torque $\mathbf{T_u}$ and the aerodynamic drag torque $\mathbf{T_d}$ can be represented as

$$\mathbf{T_u}=\mathbf{Q}^{-1}\mathbf{T_c},\ \mathbf{T_d}=\mathbf{Q}^{-1}[\mathbf{L_d}\times(\mathbf{R}^{\mathrm{T}}\mathbf{F_d})],$$

where $\mathbf{L_d}=[\,l_d^x\ \ l_d^y\ \ l_d^z\,]^T$ is the position of point of application by the aerodynamic drag $\mathbf{F_d}$ with respect to A.

D. Dynamics of ducted fan UAV

Lagrangian function of the ducted fan UAV system is given as follows:

$$L=\frac{1}{2}\mathbf{\Omega}^T\mathbf{J}\mathbf{\Omega}+\frac{1}{2}\dot{\mathbf{\Xi}}^T\mathbf{M}\dot{\mathbf{\Xi}}-\mathbf{F_g}^T\mathbf{\Xi} \tag{2}$$

where $\mathbf{M}$ =diag(m , m , m) and $\mathbf{J}$ =diag(J_1 , J_1 , J_2) are the mass and inertia matrices, respectively.

From the Lagrange-D'Alembert principle, the motion of the ducted fan UAV is described as follows:

$$\mathbf{M}\ddot{\mathbf{\Xi}}+\mathbf{F_d}+\mathbf{F_g}=\mathbf{R}\mathbf{F_c} \tag{3—1}$$

$$\mathbf{D}(\mathbf{\Theta})\ddot{\mathbf{\Theta}}+\mathbf{C}(\mathbf{\Theta},\dot{\mathbf{\Theta}})\dot{\mathbf{\Theta}}+\mathbf{T_d}=\mathbf{T_u} \tag{3—2}$$

where $\mathbf{D}$ and $\mathbf{C}$ are the inertial and coupling matrices of the attitude dynamics (3—2).

III. DECOUPLING CONTROL FRAMEWORK

Given that the elements in $\mathbf{T_u}=\mathbf{Q}^{-1}\mathbf{T_c}$ are the independent control variables ($\mathbf{Q}$ is nonsingular in the neighborhood of the upright equilibrium point $\theta=\psi\equiv 0$), the local control for the attitude may ensure system stability [7]. However, in the case of the path following, we cannot avoid a problem that the attitude dynamics and the flight dynamics share the control inputs arising from the control surface motions and highly couple with each other. This section introduces a decoupling control framework based on an attitude-guidance.

A. Analysis of Flight dynamics

The flight dynamics (3—1) can be reformulated as

$$m\ddot{x}+\upsilon_x=f_t r_{13}\triangleq u_x \tag{4—1}$$

$$m\ddot{y}+\upsilon_y=f_t r_{23}\triangleq u_y \tag{4—2}$$

$$m\ddot{z}+\upsilon_z=f_t r_{33}\triangleq u_z \tag{4—3}$$

where

$$\upsilon_x=f_x^d-f_c^x r_{11}-f_c^y r_{12}$$

$$\upsilon_y=f_y^d-f_c^x r_{21}-f_c^y r_{22}$$

$$\upsilon_z=f_z^d-f_c^x r_{31}-f_c^y r_{32}+mg$$

$$r_{13}=\cos\phi\sin\theta\cos\psi+\sin\phi\sin\psi$$

$$r_{23}=\sin\phi\sin\theta\cos\psi-\cos\phi\sin\psi$$

$$r_{33}=\cos\theta\cos\psi\ .$$

It is now clear that the propeller thrust f_t itself does not participate in the control of the lateral and longitudinal flight dynamics, but it is a "large amplification coefficient" for the attitude-dependent inputs r_{13} and r_{23}. Thus the behaviors of the attitude dynamics are considered as the inputs of the lateral and longitudinal flight dynamics. By contrast, the dynamics along the vertical direction is governed directly by the input variable $u_z = f_t r_{33}$.

B. Design of Attitude Command Generator

First, we introduce the desired attitude-dependent inputs r_{13}^d and r_{23}^d, and the pseudo control inputs of the lateral and longitudinal flight dynamics u_r^x and u_r^y, such that

$$u_r^x - u_x = \hat{f}_t r_{13}^d - f_t r_{13} \triangleq \tilde{u}_x \quad (5\text{—}1)$$

$$u_r^y - u_y = \hat{f}_t r_{13}^d - f_t r_{13} \triangleq \tilde{u}_y \quad (5\text{—}2)$$

where $\hat{f}_t$ is the nominal value of the propeller thrust f_t. Meanwhile, let them satisfy the following relations:

$$r_{13}^d = \hat{f}_t^{-1} u_r^x = \cos\phi_d \sin\theta_d \cos\psi_d + \sin\phi_d \sin\psi_d \quad (6\text{—}1)$$

$$r_{23}^d = \hat{f}_t^{-1} u_r^y = \sin\phi_d \sin\theta_d \cos\psi_d - \cos\phi_d \sin\psi_d \quad (6\text{—}2)$$

where θ_d, ψ_d, and ϕ_d are the attitude commands. Then we obtain

$$\psi_d = \arcsin(\hat{f}_t^{-1} u_r^x \sin\phi_d - \hat{f}_t^{-1} u_r^y \cos\phi_d) \quad (7\text{—}1)$$

$$\theta_d = \arcsin\left(\frac{\hat{f}_t^{-1} u_r^x \cos\varphi_d + \hat{f}_t^{-1} u_r^y \sin\varphi_d}{\sqrt{1-\sin^2\psi_d}}\right). \quad (7\text{—}2)$$

Given that the first and second derivatives of θ_d and ψ_d are unmeasurable, a third order filter, $H(s) \triangleq 1/(s+a)^3$, is considered in the following modification process:

$$\theta_r = H(s)\theta_d \quad (8\text{—}1)$$

$$\psi_r = H(s)\psi_d \quad (8\text{—}2)$$

where s is the Laplace variable, and a is the positive design parameter, which is chosen as the large value to reduce the delay-time of the filter.

Remark 1: When the error between $\hat{f}_t$ and f_t is small and the performance in the attitude commands tracking is ensured to be high trough the control torque $\mathbf{T_u}$, we have $\theta_d \cong \theta_r \cong \theta$, $\psi_d \cong \psi_r \cong \psi$, $\phi_d \cong \phi$, $\tilde{u}_x \cong 0$, and $\tilde{u}_y \cong 0$. In this situation, the lateral and longitudinal flight dynamics are represented as $m\ddot{x} + \upsilon_x \cong u_r^x$ and $m\ddot{y} + \upsilon_y \cong u_r^y$, respectively. This shows that the attitude dynamics and the lateral and longitudinal flight dynamics can be governed by the control torque $\mathbf{T_u}$ and the pseudo control inputs u_r^x and u_r^y, respectively.

IV. Robust Adaptive Control Design

As previously mentioned, the theories on robust adaptive control and neural network control are reliable and efficient in the compensation of the unknown disturbances, but theses schemes cause a relatively complex algorithm structure. This section presents a compensation method based on the system function approximation.

A. System Function Approximation

Given the desired paths $\mathbf{\Xi_d} = [\, x_d \;\; y_d \;\; z_d \,]^{\mathrm{T}}$ and the attitude commands $\mathbf{\Theta_d} = [\, \theta_r \;\; \psi_r \;\; \phi_d \,]^{\mathrm{T}}$, the corresponding tracking errors are $\mathbf{e_1} = \mathbf{\Xi_d} - \mathbf{\Xi}$ and $\mathbf{e_2} = \mathbf{\Theta_r} - \mathbf{\Theta}$, as well as the filtered tracking errors are

$$\boldsymbol{\xi}_1 = \mathbf{\Lambda}_1 \mathbf{e}_1 + \dot{\mathbf{e}}_1 \triangleq \left[\, \xi_x \;\; \xi_y \;\; \xi_z \,\right]^T$$

$$\boldsymbol{\xi}_2 = \mathbf{\Lambda}_2 \mathbf{e}_2 + \dot{\mathbf{e}}_2 \triangleq \left[\, \xi_\theta \;\; \xi_\psi \;\; \xi_\phi \,\right]^T$$

where $\mathbf{\Lambda_1} > 0$ and $\mathbf{\Lambda_2} > 0$ are the design parameter matrices. The flight dynamics (4) and the attitude dynamics (3—2) can then be written in terms of the filtered tracking errors as

$$\mathbf{M}\dot{\boldsymbol{\xi}}_1 = \mathbf{M}\boldsymbol{\zeta}_1 + \mathbf{F_d^v} - \mathbf{F_u} \quad (9\text{—}1)$$

$$\mathbf{D}\dot{\boldsymbol{\xi}}_2 = \mathbf{D}\dot{\boldsymbol{\zeta}}_2 + \mathbf{C}\boldsymbol{\zeta}_2 + \mathbf{T_d} - \mathbf{C}\boldsymbol{\xi}_2 - \mathbf{T_u} \quad (9\text{—}2)$$

where $\mathbf{F_u} = [\, u_r^x \;\; u_r^y \;\; u_z \,]^T$, $\mathbf{F_d^v} = [\, \upsilon_x + \tilde{u}_x \;\; \upsilon_y + \tilde{u}_y \;\; \upsilon_z + mg \,]^T$, $\boldsymbol{\zeta}_1 = \dot{\mathbf{\Xi}}_\mathbf{d} + \mathbf{\Lambda}_1 \mathbf{e}_1$, and $\boldsymbol{\zeta}_2 = \dot{\mathbf{\Theta}}_\mathbf{d} + \mathbf{\Lambda}_2 \mathbf{e}_2$.

Assumption: In the Equation (9), the each element of the system function vectors, $\mathbf{\Delta_1} = \mathbf{M}\boldsymbol{\zeta}_1 + \mathbf{F_d^v} \triangleq [\, \delta_x \;\; \delta_y \;\; \delta_z \,]^T$ and $\mathbf{\Delta_2} = \mathbf{D}\dot{\boldsymbol{\zeta}}_2 + \mathbf{C}\boldsymbol{\zeta}_2 + \mathbf{T_d} \triangleq [\, \delta_\theta \;\; \delta_\psi \;\; \delta_\phi \,]^T$, is composed of the low and high frequency components and restricted to the following compact sets:

$$S_1 = \{(\boldsymbol{\chi}_1,\ \mathbf{F_d^v}) \mid \|\boldsymbol{\chi}_1\| < b_1^\chi,\ \left\|\mathbf{F_d^v}\right\| < \varpi_1\} \quad (10\text{—}1)$$

$$S_2 = \{(\boldsymbol{\chi}_2,\ \mathbf{T_d}) \mid \|\boldsymbol{\chi}_2\| < b_2^\chi,\ \left\|\mathbf{T_d}\right\| < \varpi_2\} \quad (10\text{—}2)$$

where $\boldsymbol{\chi}_1 = [\, \mathbf{e}_1^T \;\; \dot{\mathbf{e}}_1^T \;\; \mathbf{\Xi}_\mathbf{d}^T \;\; \dot{\mathbf{\Xi}}_\mathbf{d}^T \;\; \ddot{\mathbf{\Xi}}_\mathbf{d}^T \,]^T$ and $\boldsymbol{\chi}_2 = [\, \mathbf{e}_2^T \;\; \dot{\mathbf{e}}_2^T \;\; \mathbf{\Theta}_\mathbf{d}^T \;\; \dot{\mathbf{\Theta}}_\mathbf{d}^T \;\; \ddot{\mathbf{\Theta}}_\mathbf{d}^T \,]^T$. This hypothesis is acceptable because the ducted fan UAV is a real physical system and each physical element in the system function vectors $\mathbf{\Delta}_1$ and $\mathbf{\Delta}_2$ itself contains the low and high frequency components.

It is easy to check from (10) that, for each time t, $\boldsymbol{\chi}_1(t)$ and $\boldsymbol{\chi}_2(t)$ are bounded by [8]

$$\left\|\boldsymbol{\chi}_j\right\| \le c_1^j + c_2^j \left\|\boldsymbol{\xi}_j\right\| \le q_j^r + c_0^j \left\|\boldsymbol{\xi}_j(0)\right\| + c_2^j \left\|\boldsymbol{\xi}_j\right\|, j=1, 2, \quad (11)$$

for computable positive constants c_0^j, c_1^j, and c_2^j, where

$$\left\|\left[\, \Xi_d^T \;\; \dot{\Xi}_d^T \;\; \ddot{\Xi}_d^T \,\right]^T\right\| \le q_1^r,\ \left\|\left[\, \Theta_d^T \;\; \dot{\Theta}_d^T \;\; \ddot{\Theta}_d^T \,\right]^T\right\| \le q_2^r.$$

Consequently, the sets of the allowable initial filtered tracking errors are represented as follows:

$$S_j^r=\{\,\xi_j \mid \|\xi_j\|<(b_j^\chi-q_j^r)\big/(c_0^j+c_2^j)\,\},\ j=1,\ 2. \qquad (12)$$

Given that $\mathbf{\Delta}_1$ and $\mathbf{\Delta}_2$ are bounded, for any given $\varepsilon_j>0$ and $\xi_1\in S_j^r$, there exists the three-dimensional weight vectors, $\mathbf{\Pi}_j$ and $\mathbf{W}_j$, such that

$$\mathbf{\Delta}_j=\mathbf{\Pi}_j+\mathbf{\Phi}_j(\xi_j)\mathbf{W}_j+\mathbf{E}_j,\ \left\|\mathbf{E}_j\right\|<\varepsilon_j,\ j=1,\ 2, \qquad (13)$$

where $\mathbf{\Phi}_1(\xi_1)$=diag[$\sigma(\mu_1\xi_x)$, $\sigma(\mu_1\xi_y)$, $\sigma(\mu_1\xi_z)$],

$\mathbf{\Phi}_2(\xi_2)$=diag[$\sigma(\mu_2\xi_\theta)$ $\sigma(\mu_2\xi_\psi)$ $\sigma(\mu_2\xi_\phi)$];

and $\sigma(\bullet)$ is the smooth saturation function defined by

$$\sigma(\mu\vartheta)=(1-e^{-\mu\vartheta})\big/(1+e^{-\mu\vartheta})$$

with a positive design parameter μ and a argument ϑ.

Remark 2: We incorporated the uncertain disturbances $\mathbf{F_d^v}$ and $\mathbf{T_d}$ into the system functions $\mathbf{\Delta_1}$ and $\mathbf{\Delta_2}$, respectively, and considered these system functions as the functions composed of the low frequency components ($\mathbf{\Pi}_j$) and the high frequency components ($\mathbf{\Phi}_j\mathbf{W}_j$). This modeling approach is beneficial for the simplification of the algorithm structure of controller.

B. Tuning Algorithm

From above analysis, the control law can be written as

$$\mathbf{F_u}=\mathbf{K}_1\xi_1+\hat{\mathbf{\Delta}}_1 \qquad (14\text{—}1)$$

$$\mathbf{T_u}=\mathbf{K}_2\xi_2+\hat{\mathbf{\Delta}}_2 \qquad (14\text{—}2)$$

where $\hat{\mathbf{\Delta}}_1=\hat{\mathbf{\Pi}}_1+\mathbf{\Phi}_1(\xi_1)\hat{\mathbf{W}}_1$ and $\hat{\mathbf{\Delta}}_2=\hat{\mathbf{\Pi}}_2+\mathbf{\Phi}_2(\xi_2)\hat{\mathbf{W}}_2$ are the estimations for $\hat{\mathbf{\Delta}}_1$ and $\hat{\mathbf{\Delta}}_2$, respectively; $\hat{\mathbf{\Pi}}_1$, $\hat{\mathbf{\Pi}}_2$, $\hat{\mathbf{W}}_1$, and $\hat{\mathbf{W}}_2$ are the estimations for $\mathbf{\Pi}_1$, $\mathbf{\Pi}_2$, $\mathbf{W}_1$, and $\mathbf{W}_2$, respectively; and $\mathbf{K}_1>0$ and $\mathbf{K}_2>0$ are the gain matrices.

From (13) and (14), the filtered tracking error dynamics is reformulated as

$$\mathbf{M}\dot{\xi}_1=-\mathbf{K}_1\xi_1+\tilde{\mathbf{\Pi}}_1+\mathbf{\Phi}_1(\xi_1)\tilde{\mathbf{W}}_1+\mathbf{E}_1 \qquad (15\text{—}1)$$

$$\mathbf{D}\dot{\xi}_2=-(\mathbf{K}_2+\mathbf{C})\xi_2+\tilde{\mathbf{\Pi}}_2+\mathbf{\Phi}_2(\xi_2)\tilde{\mathbf{W}}_2+\mathbf{E}_2 \qquad (15\text{—}2)$$

where $\tilde{\mathbf{\Pi}}_j=\mathbf{\Pi}_j-\hat{\mathbf{\Pi}}_j$, and $\tilde{\mathbf{W}}_j=\mathbf{W}_j-\hat{\mathbf{W}}_j$ (j=1, 2).

Lemma: Assume $\mathbf{\Pi}_j$ and $\mathbf{W}_j$ are constant and bounded by $\left\|\mathbf{\Pi}_j\right\|\le\pi_j$ and $\left\|\mathbf{W}_j\right\|\le w_j$ (j=1, 2). Let the control inputs $\mathbf{F_u}$ and $\mathbf{T_u}$ be given by (14) and the control gain

$$K_{j\min}>\frac{(\alpha_j\pi_j^2+\beta_j w_j^2+4\varepsilon_j)(c_0^j+c_2^j)}{4(b_j^\chi-q_j^r)} \qquad (16)$$

where α_j and β_j are the small positive design parameters. Let $\mathbf{\Pi}_j$ and $\mathbf{W}_j$ be estimated respectively by the following state variable integral and saturation function:

$$\dot{\hat{\mathbf{\Pi}}}_j=\mathbf{F}_j\xi_j-\alpha_j\mathbf{F}_j\left\|\xi_j\right\|\hat{\mathbf{\Pi}}_j \qquad (17\text{—}1)$$

$$\dot{\hat{\mathbf{W}}}_j=\mathbf{H}_j\mathbf{\Phi}_j(\xi_j)\xi_j-\beta_j\mathbf{H}_j\left\|\xi_j\right\|_j\hat{\mathbf{W}}_j \qquad (17\text{—}2)$$

with $\mathbf{F}_j=\mathbf{F}_j^T>0$ and $\mathbf{H}_j=\mathbf{H}_j^T>0$. Then, ξ_j, $\tilde{\mathbf{\Pi}}_j$, and $\tilde{\mathbf{W}}_j$ are uniformly and ultimately bounded with practical bounds given respectively by the right-hand sides of (18) and (19).

Proof: According to the train of thought of the proof in [8], we define the Lyapunov function candidate as

$$V=\frac{1}{2}\sum_{j=1}^{2}\tilde{\mathbf{\Pi}}_j^T\mathbf{F}_j^{-1}\tilde{\mathbf{\Pi}}_j+\frac{1}{2}\sum_{j=1}^{2}\tilde{\mathbf{W}}_j^T\mathbf{H}_j^{-1}\tilde{\mathbf{W}}_j$$
$$+\frac{1}{2}\xi_1^T\mathbf{M}\xi_1+\frac{1}{2}\xi_2^T\mathbf{D}\xi_2$$

Differentiating yields

$$\dot{V}=\sum_{j=1}^{2}\tilde{\mathbf{\Pi}}_j^T\mathbf{F}_j^{-1}\dot{\tilde{\mathbf{\Pi}}}_j+\sum_{j=1}^{2}\tilde{\mathbf{W}}_j^T\mathbf{H}_j^{-1}\dot{\tilde{\mathbf{W}}}_J$$
$$+\xi_1^T\mathbf{M}\dot{\xi}_1+\xi_2^T\mathbf{D}\dot{\xi}_2+\frac{1}{2}\xi_2^T\dot{\mathbf{D}}\xi_2$$

and substituting (15) yields

$$\dot{V}=\sum_{j=1}^{2}\xi_j^T\left[-\mathbf{K}_j\xi_j+\tilde{\mathbf{\Pi}}_j+\mathbf{\Phi}_j(\xi_j)\tilde{\mathbf{W}}_j+\mathbf{E}_j\right]$$
$$+\sum_{j=1}^{2}\tilde{\mathbf{\Pi}}_j^T\mathbf{F}_j^{-1}\dot{\tilde{\mathbf{\Pi}}}_j+\sum_{j=1}^{2}\tilde{\mathbf{W}}_j^T\mathbf{H}_j^{-1}\dot{\tilde{\mathbf{W}}}_j$$

Here, applying tuning law (17) yields

$$\dot{V}=\sum_{j=1}^{2}\beta_j\left\|\xi_j\right\|\tilde{\mathbf{W}}_j^T\left(\mathbf{W}_j-\tilde{\mathbf{W}}_j\right)$$
$$+\sum_{j=1}^{2}\alpha_j\left\|\xi_j\right\|\tilde{\mathbf{\Pi}}_j^T\left(\mathbf{\Pi}_j-\tilde{\mathbf{\Pi}}_j\right)$$
$$+\sum_{j=1}^{2}\xi_j^T\left(-\mathbf{K}_j\xi_j+\mathbf{E}_j\right)$$

Since

$$\tilde{\mathbf{\Pi}}_j^T\left(\mathbf{\Pi}_j-\tilde{\mathbf{\Pi}}_j\right)\le\pi_j\left\|\tilde{\mathbf{\Pi}}_j\right\|-\left\|\tilde{\mathbf{\Pi}}_j\right\|^2,$$

$$\tilde{\mathbf{W}}_j^T\left(\mathbf{W}_j-\tilde{\mathbf{W}}_j\right)\le w_j\left\|\tilde{\mathbf{W}}_j\right\|-\left\|\tilde{\mathbf{W}}_j\right\|^2,$$

results in

$$\dot{V}\le-\sum_{j=1}^{2}\left\|\xi_j\right\|\left[\begin{array}{l}\alpha_j\left(\left\|\tilde{\mathbf{\Pi}}_j\right\|-\dfrac{\pi_j}{2}\right)^2+\beta_j\left(\left\|\tilde{\mathbf{W}}_j\right\|-\dfrac{w_j}{2}\right)^2\\ +K_{j\min}\left\|\xi_j\right\|-\dfrac{\alpha_j\pi_j^2+\beta_j w_j^2+4\varepsilon_j}{4}\end{array}\right],$$

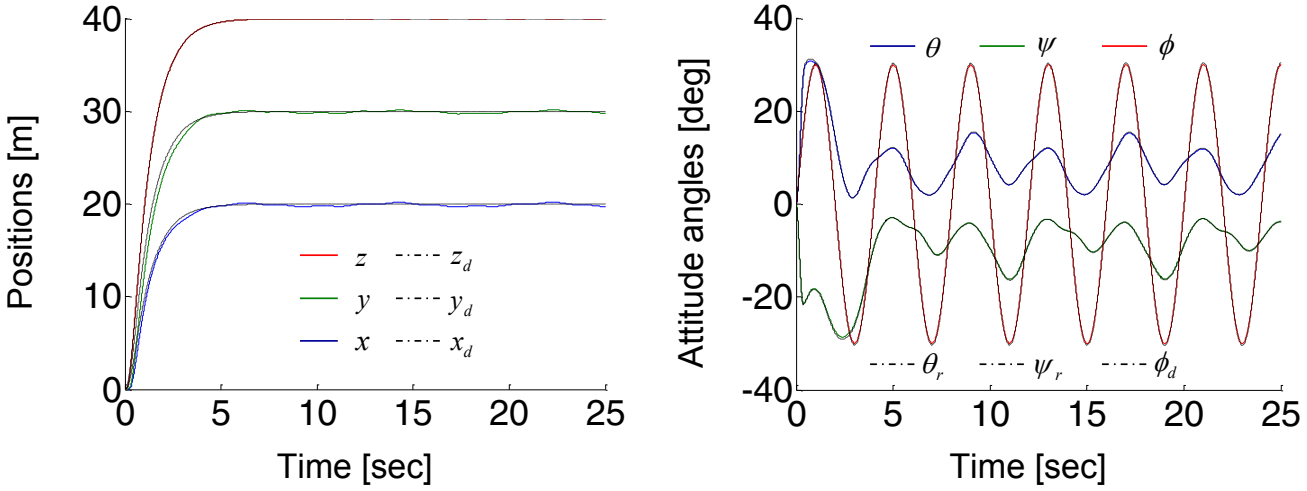

Fig. 2 Results of path following control and the attitude command tracking under the step path.

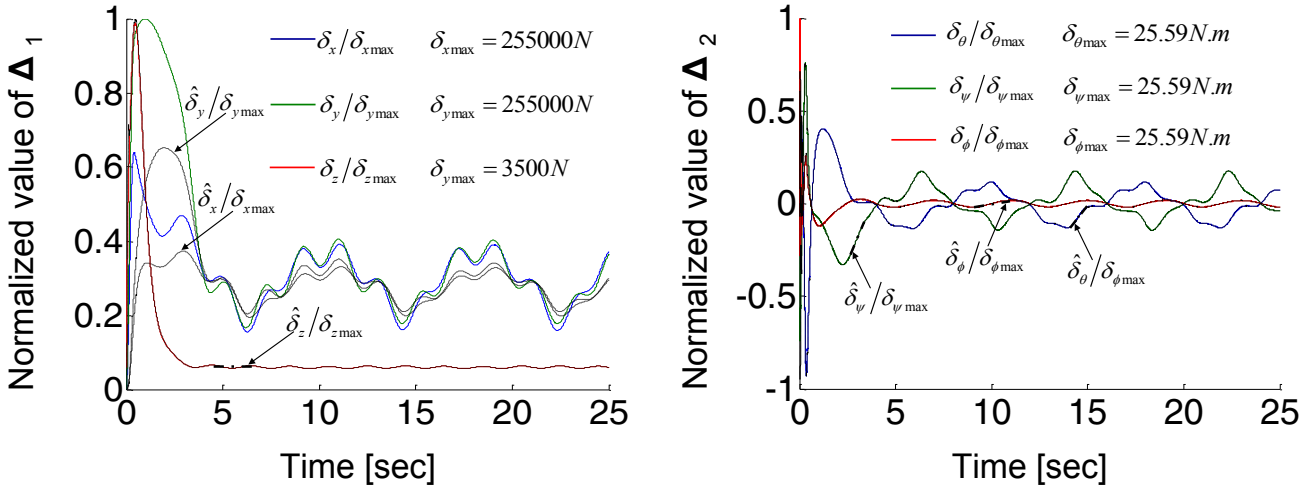

Fig. 3 Results of the system function estimation.

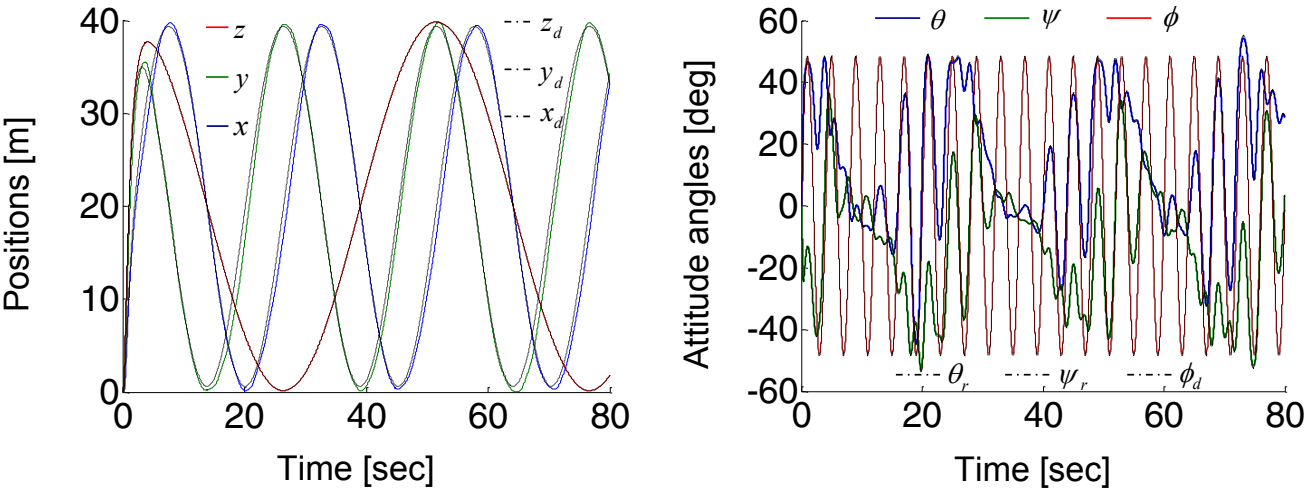

Fig. 4 Results of path following control and the attitude command tracking under the circle path.

which is negative as long as

$$\left\|\boldsymbol{\xi}_j\right\| > \frac{\alpha_j \pi_j^2 + \beta_j w_j^2 + 4\varepsilon_j}{4K_{j\min}} \equiv b_\xi^j \tag{18}$$

or

$$\left\|\tilde{\boldsymbol{\Pi}}_j\right\| > \frac{\pi_j}{2} + \sqrt{\frac{\pi_j^2}{4} + \frac{\varepsilon_j}{2\alpha_j}} \equiv b_\pi^j \tag{19—1}$$

$$\left\|\tilde{\mathbf{W}}_j\right\| > \frac{w_j}{2} + \sqrt{\frac{w_j^2}{4} + \frac{\varepsilon_j}{2\beta_j}} \equiv b_w^j . \tag{19—2}$$

Obviously, $\dot{V}$ is negative outside the compact sets $\left\|\boldsymbol{\xi}_j\right\| \le b_\xi^j$, $\left\|\tilde{\boldsymbol{\Pi}}_j\right\| \le b_\pi^j$, and $\left\|\tilde{\mathbf{W}}_j\right\| \le b_w^j$. This illustrates uniform ultimate boundedness of $\boldsymbol{\xi}_j$, $\tilde{\boldsymbol{\Pi}}_j$, and $\tilde{\mathbf{W}}_j$. Selecting the gain $K_{j\min}$ according to (16) ensures that the sets defined by $\left\|\boldsymbol{\xi}_j\right\| \le b_\xi^j$ is contained in S_j^r. Therefore, the approximation property (13) holds for given compact sets S_j in (10).

V. Simulation Verification

In this section, we present simulation results to illustrate the convergence properties shown in lemma. Parameters of the model (3) were chosen as:

$$m = 17\ \ kg,\ J_1 = 0.883\ \ kg.m^2,\ J_2 = 0.3137\ \ kg.m^2,$$

$$l_1 = 0.3716\ \ m,\ l_2 = 0.1625\ \ m,\ g = 9.8\ \ m/sec^2.$$

The aerodynamic interferences were set as

$c_x = c_y = c_z = 3.5\ N/m^2/sec^2$, $v_x = \dot{x} + 3 + 0.5\sin \pi t\ \ m/sec$,

$v_y = \dot{y} + 3 + 0.5\sin \pi t\ \ m/sec$, $v_z = \dot{z} + 3 + 0.5\sin \pi t\ \ m/sec$,

$$l_d^x = l_d^y = l_d^z = 0.1\sin 0.25\pi t\ \ m .$$

The control algorithm has been run with the following design parameters. **(a)** Command generators: $\hat{f}_t^{-1} = 2\times 10^{-6}$, $a = 471$; **(b)** Saturation functions: $\mu_1 = 0.25$, $\mu_2 = 35$; **(c)** Controller gains: $\mathbf{K}_1$ =diag(9568, 9568, 47), $\mathbf{K}_2$ =diag(30, 30, 30), $\boldsymbol{\Lambda}_1 = \boldsymbol{\Lambda}_2$ =diag(3, 3, 3); **(d)** Adaptive tuning algorithms: $\mathbf{F}_2 = \mathbf{H}_2$ =diag(979, 979, 979), $\mathbf{F}_1 = \mathbf{H}_1$ =diag(9792, 9792, 9792), $\alpha_1 = \alpha_2 = \beta_1 = \beta_2 = 10^{-5}$.

Fig. 2 illustrates the ability of the proposed decoupling control framework to coordinate the mutual interference between the attitude dynamics and the flight dynamics in the process of the path following. The ducted fan UAV exactly follows the desired path (left figure) by the attitude control (right figure), even though the strong nonlinear couplings and aerodynamic interferences exist.

Fig. 3 compares the real system functions $\boldsymbol{\Delta}_1$ and $\boldsymbol{\Delta}_2$ (solid lines) with their estimations $\hat{\boldsymbol{\Delta}}_1$ and $\hat{\boldsymbol{\Delta}}_2$ (dashed black lines) computed by using the tuning algorithm (17). The fast and correct convergences demonstrate that our proposed approach is effective to attenuate the adverse effects of the unknown external disturbances.

The results of the path following control and the attitude command tracking under the circle motion are shown in the Fig. 4. Despite the change in the operating condition, the ducted fan UAV tracks the desired path (left figure) well by the attitude adjustment (right figure).

VI. Conclusion

We have established a mapping model between the attitude commands and the pseudo control inputs of the lateral and longitudinal flight dynamics to realize an attitude-guided path following control. Advantage of this modeling approach lies in its coordination function that allows the attitude controller and the flight controller to be designed individually without mutual interference and enables the ducted fan UAV to track the desired path well under the presence of the yaw motion. A system function (disturbance) estimation method based on the state variable integral and the smooth saturation function has been proposed to simplify the control algorithm structure, and the less performance degradation of the controller, under the presence of the unknown disturbances, have been obtained. Uniform ultimate boundedness of the closed-loop dynamics of ducted fan UAV has been proved and demonstrated via the numerical simulations.

Future works are summarized as follows: the performance in the path following control is limited when the rate of variation of the position commands become larger. Therefore, the further research for enlarging the bandwidth of the pseudo control of the lateral and longitudinal flight dynamics should be done. Furthermore, the comparison and the analysis of the several control technologies including adaptive control and neural-network-based intelligent control are also important for future work.

References

[1] Osgar John Ohanian III, "Ducted Fan Aerodynamics and Modeling, with Applications of Steady and Synthetic Jet Flow Control," Ph.D thesis, Virginia Polytechnic Institute and State University, USA, 2011.

[2] Lorenzo Marconi and Roberto Naldi, "Control of Aerial Robots: Hybrid Force and Position Feedback for a Ducted Fan," IEEE Control Systems Magazine, Aug. 2012.

[3] C. M. Spaulding, M. H. Nasur, M. B. Tischler, R. A. Hess, and J. A. Franklin, "Nonlinear Inversion Control for a Ducted Fan UAV," AIAA Atmospheric Flight Mechanics Conference and Exhibit, San Francisco, California, 15-18 Aug. 2005.

[4] W. MacKunis, P.M. Patre, M.K. Kaiser, and W.E. Dixon, "Asymptotic Tracking for Aircraft via Robust and Adaptive Dynamic Inversion Methods," IEEE Transactions on Control Systems Technology, vol. 18, no. 6, pp. 1448-1456, Nov. 2010.

[5] E.N. Johonson and M.A. Turbe, "Modeling, Control and Flight Testing of a Small Ducted Fan Aircraft," Journal of guidance, control, and dynamics, 29(4):769–779, 2006.

[6] Jean Michel Pflimlin, Philippe Sou`eres, and Tarek Hamel, "Hovering-flight Stabilization in Wind Gusts for Ducted Fan UAV," 43rd IEEE Conference on Decision and Control, Atlantis, Dec. 2004.

[7] Jean Michel Pflimlin, Tarek Hamel, Philippe Soueres, and Robert Mahony, "A Hierarchical Control Strategy for the Autonomous Navigation of a Ducted Fan Flying Robot," Proceedings of the 2006 IEEE International Conference on Robotics and Automation, Orlando, Florida, May 2006.

[8] K.S.Narendra and A.M.Annaswamy, "A new adaptive law for robust adaptive control without persistent excitation," IEEE Trans. Automat. Control, vol. 32, pp. 134–145, Feb., 1987.